Journal of *Marine Science and Engineering*

MDPI

Article

Dynamic Response of a SPAR-Type Floating Wind Turbine Foundation with Taut Mooring System

Gong Xiang [1,2], Xianbo Xiang [1,2,*] and Xiaochuan Yu [3]

[1] School of Naval Architecture and Ocean Engineering, Huazhong University of Science and Technology, Wuhan 430074, China
[2] Hubei Key Laboratory of Naval Architecture and Ocean Engineering Hydrodynamics (HUST), Wuhan 430074, China
[3] School of Naval Architecture and Marine Engineering, University of New Orleans, New Orleans, LA 70148, USA
* Correspondence: xbxiang@hust.edu.cn

Abstract: Compared with the traditional catenary or semi-taut mooring lines, the taut mooring system is more advantageous in many aspects, such as reduction of mooring line loads, erosion and fatigue damage during the powering productions of the floating wind turbines. This paper presents a taut mooring system made of synthetic fiber mooring lines, which can experience large elongations for a spar-type floating wind turbine. A finite element method (FEM)-based tensile mooring line model is proposed to study the mooring statics and dynamics of the floating wind turbine. A time domain modelling method coupled with the developed mooring line model is adopted to study the dynamics of a spar-type floating wind turbine foundation moored by the taut mooring system under regular waves. A systematic dynamic response and structural analysis are conducted based on variations in the mooring length and pretension. Additionally, comparative performance analyses are investigated for two mooring configurations with different numbers of mooring lines: two-point and three-point taut mooring system. It is found that factors, such as mooring length, pretension and the number of mooring lines, have significant impact on the in-plane and out-of-plane motion responses of the foundation.

Keywords: spar-type floating wind turbine; taut mooring system; FEM; tensile mooring line; dynamic response; mooring configurations

Citation: Xiang, G.; Xiang, X.; Yu, X. Dynamic Response of a SPAR-Type Floating Wind Turbine Foundation with Taut Mooring System. *J. Mar. Sci. Eng.* **2022**, *10*, 1907. https://doi.org/10.3390/jmse10121907

Academic Editors: Shan Wang, Philipp R. Thies, Yushun Lian and Carlos Guedes Soares

Received: 12 November 2022
Accepted: 1 December 2022
Published: 5 December 2022

1. Introduction

In the past decades, an increasing number of floating marine systems have been designed, produced and operated in the sea to adhere to the demand of exploring the ocean energy resources deeper and further away from the land [1–5]. The typical floating systems for harvesting ocean resources include traditional oil and gas platforms [2,6,7], as well as renewable energy devices, such as wind turbines, tidal/current turbines, wave energy converters and their associated operational systems [4,8–10].

There are three main types of mooring design for floating wind turbines: the catenary mooring system, semi-taut mooring system and taut mooring system. Most of the mooring systems under operations are catenary or semi-taut. Several catenary mooring configurations were proposed that could be accomplished with single or multi-connections [1]. Astariz and Iglesias [11] found the most appropriate mooring was CALM (catenary anchor leg mooring), which has the advantages of easy installation, lower cost and less effects of corrosions. However, the use of catenaries may suffer from wear and fatigue damage and affect the structure safety due to vortex-induced vibration. Gao and Moan [12] also pointed out that a catenary line system usually consisting of chain links relies on the weight of links or clump weights to provide horizontal restoring force. If no clump weight is used, a very long mooring line of chain links must be considered to obtain adequate flexibility.

Furthermore, catenary line systems will bring large, vertically downward loads to the floating structures. This could limit the allowable deck loads for floating wind turbines. Therefore, this concept might not be suitable in shallow waters.

As shown in Figure 1, with synthetic fibers becoming very promising mooring materials, the taut mooring system is treated as a good alternative of mooring system for floating wind turbines. The possible new materials, such as AI foam, might also be able to be used for the composition of the mooring lines after enhancement of the structural strength. The diameter sizes of those synthetic fiber ropes used for commercial purposes vary within the range of 16 mm to 240 mm [13] and are typically made of nylon (polyamide), polyester (polyethylene terephthalate), aramid (para-aramid), or HMPE (high-modulus polyethylene). Synthetic fiber ropes are significantly lighter than other materials and, therefore, can be used in the water column of a taut mooring system. Casaubieilh [14] found that the new generation of mooring system, taut configuration using tether mooring lines, can significantly reduce the loads on mooring lines, floating structure and anchors, and it can also reduce the device excursions when comparing to the conventional catenary moorings. The elastic properties of fiber ropes are also of interest to damp mooring loads, and they avoid snap loads [13].

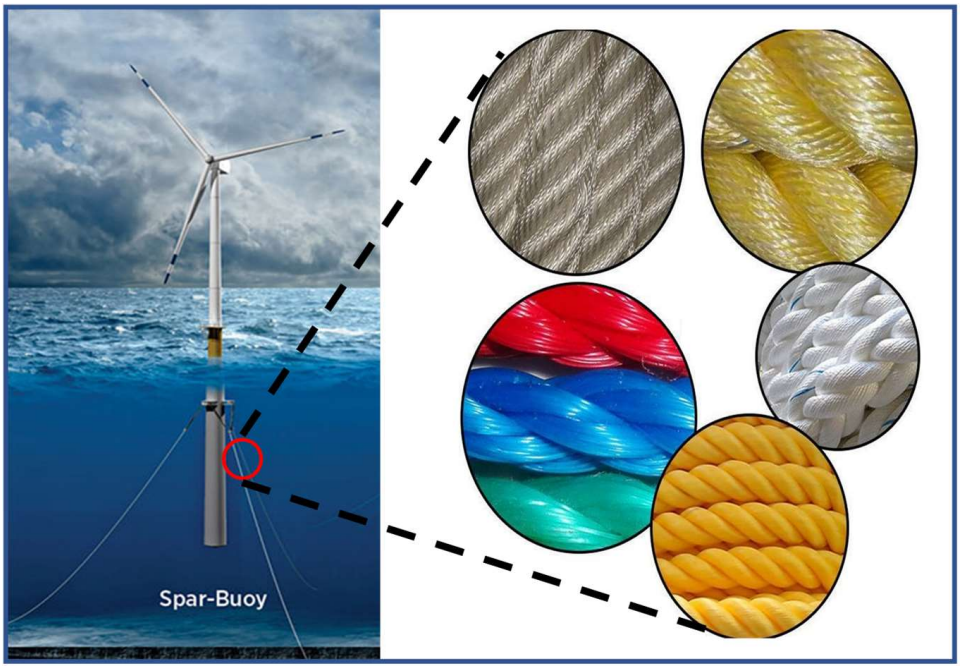

Figure 1. Synthetic fibers applied into the taut mooring system of floating wind turbine.

The nonlinear time-dependent mechanical properties of the taut mooring lines, such as synthetic fiber ropes, are found to be very complex [15,16]. Therefore, how to deal with the dynamics of the whole floating system composed by the floating structure and fiber ropes also becomes a complicated problem. Before the late 20th century, the oscillatory motion of floating structures was calculated without considering the dynamic response of the mooring cables and a linearized stiffness reaction from their mooring systems was presumed. This is the so-called quasi-static mooring analysis. However, for moored floating renewables, especially floating wind turbines and wave energy converters in shallow water, it has been pointed out lately that the mooring design must be an integral part of the whole floating system design [17], as the mooring design can significantly influence the behaviors of the floating structures, the operations, the survival and maintenance. As a result of all the above, there is a great need for an accurate understanding of the dynamics of floating wind turbines coupled with the responses from fiber rope mooring lines and an accurate analysis of the body motion responses and the mooring tension of the associated mooring system.

Currently, many researchers have managed to experimentally investigate the dynamic performance of the floating renewables, such as floating wind turbines and wave energy converters with the taut mooring system, to disclose their coupling dynamic effects [18,19]. However, how to numerically solve the dynamic responses from fiber rope mooring lines is a critical problem during coupling analysis between floating structure and mooring lines. Fortunately, there has been some existing knowledge to use in the past decades. Researchers have established several frequency or time-domain modelling methods to consider the dynamics of traditional taut mooring lines, such as chains, steel wires, springs, etc., to couple with the floaters. The main time domain modelling approaches used for mooring dynamic analysis usually involve different spatial and temporal discretization methods based on either a lumped-mass model (LMM) [19–22] or slender rod model solved by either finite difference method (FDM) [23,24] or finite element method (FEM) [25–28]. These mooring dynamic models can also be applied into new taut mooring lines, such as fiber ropes. However, compared with chains and steel wires, fiber ropes usually suffer much larger elongations; thus, mooring dynamic models used for studying the dynamics of fiber ropes may also be required to change somehow. Currently, there is little research into the dynamics of the fiber ropes. Generally, the fiber rope mooring line is treated as having a constant storm stiffness in the calculations, considering the mooring line tension is the targeted parameter to be calculated as the interface between floating structure and fiber rope mooring lines. Thomsen et al. [19] utilized LMM-based software, Orcaflex, to simulate a three-legged turret mooring system with synthetic lines for a wind/wave energy converter, known as a floating power plant. Generally, good agreement was found for the tensions in the lines. Nguyen et al. [29] simplified the mooring line as a vertical elastic spring-mass system with a constant stiffness when studying the hydro-elastic responses of pontoon-type VLFS moored by vertical elastic lines. Xiong et al. [30,31] developed a dynamic method using the LMM to study the dynamics of the elastic mooring chain, which suffers large elongations under deep water by considering the soil–chain interaction for the embedded anchor chain. Qiao et al. [32] conducted the dynamic finite element analysis of the taut mooring lines with chain–polyester–chain segments to investigate the slack–taut phenomenon. Because of many advantageous factors, including coding simplicity, computational efficiency, and earlier applications as a design and analysis tool, LMM is more widely used in the above studies. However, LMM is actually a simplified form with the order reduction of the FEM-based process. Depending on the implementation used, LMM formulations generally require many more elements to reach the similar accuracy of FEM assemblies. When comparing FDM with FEM, FEM can guarantee L2 stability using the Galerkin method, while FDM will not work if finite-differencing schemes are paired with incompatible integration techniques. Additionally, compared with the LMM and FEM, FDM are inherently more prone to numerical errors or drifts because the FDM formulation does not guarantee the conservation of energy.

This paper presents a time domain modelling method to study the dynamics of a spar-type floating wind turbine moored by the synthetic fiber mooring lines under regular waves. The simulations of motion response and the tension force on the mooring lines at the fairlead of the foundation with a three-point (T3) taut mooring system under regular waves are studied using traditional stiff and proposed tensile mooring line model. The dynamics of a spar-type floating wind turbine foundation moored by synthetic fiber mooring lines of different lengths and pretensions have been simulated. Comparative performance analysis of two-point (T2) and three-point (T3) taut mooring systems are also conducted. In a nutshell, the main contributions of the present work are:

(1) To overcome the drawbacks of the stiff mooring line model when calculating the dynamics of synthetic fiber ropes, am FEM formulation of tensile mooring line model is proposed to be capable of studying the statics and dynamics of tensile mooring lines experiencing large elongations.

(2) By integrating the tensile mooring line model and the Morison forces into the equations of motion, a time domain modelling code is developed to study the coupled dynamics of spar-type floating wind turbine foundation moored by synthetic fiber ropes.
(3) The effects of the taut mooring system configurations on the dynamic responses of a spar-type floating wind turbine foundation and the loads on the synthetic fiber mooring lines have been systematically investigated via changing mooring lengths and pretensions; the number of mooring lines: T2 and T3.

2. Methodology

2.1. Dynamics of a Tensile Mooring Line

The mooring line is generally treated as a slender rod when studying its dynamics. In a 3D Cartesian coordinate system, the rod is expressed as a function of time t and the arc length s along the rod, namely a position vector, $\mathbf{r}(s, t)$, as shown in Figure 2. In Figure 2, the unit vectors in tangential, normal and binormal directions are expressed by **t**, **n** and **b**, respectively. The rod tensile is usually assumed to allow for large axial elongation; the original arc length is s while the deformed arc length is $\overline{S}$ as shown in Figure 2.

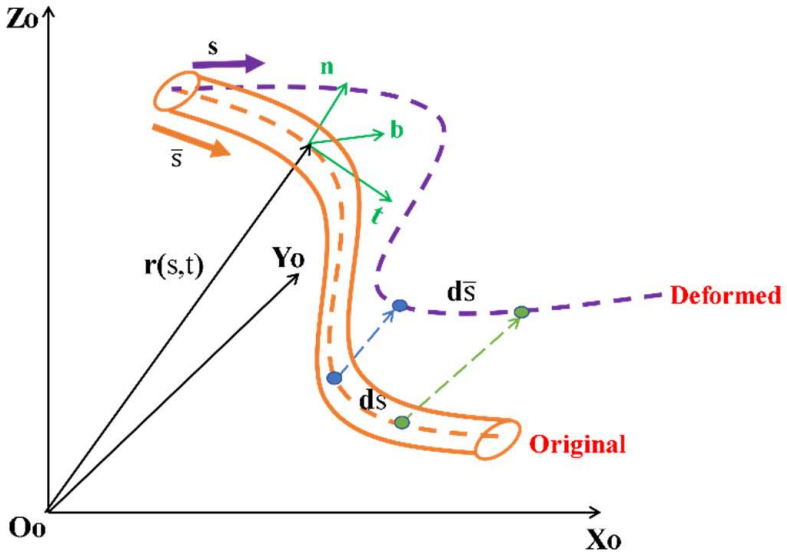

Figure 2. The rod in original and deformed state.

For a slender rod, the equations of motion are developed based on general conservation of linear momentum and moment of momentum [33,34] and can be expressed as

$$\widetilde{\mathbf{M}}' + \mathbf{r}' \times \mathbf{F} + \mathbf{m} = 0 \tag{1}$$

$$\mathbf{F}' + \mathbf{q} = \rho\ \ddot{\mathbf{r}}(s, t) \tag{2}$$

where, **q** is the external load acting on the rod per unit length, ρ and **m** is the mass and the external moment per unit length, respectively. The symbol of prime indicates the space derivative with respect to s, while the symbol of superposed dot represents time derivative. Correspondingly, **F** is the total force acting at a point while $\widetilde{\mathbf{M}}$ **is** the total moment acting at the centerline of the rod.

Based on the Bernoulli–Euler theory, the related total moment $\widetilde{\mathbf{M}}$ can be expressed by

$$\widetilde{\mathbf{M}} = \mathbf{r}' \times (B\mathbf{r}'') + H\mathbf{r}' \tag{3}$$

By merging Equations (2) and (3), the equations of motion of slender rod are represented by

$$\mathbf{r}' \times (B\mathbf{r}'')' + H'\mathbf{r}' + H\mathbf{r}'' + \mathbf{r}' \times \mathbf{F} + \mathbf{m} = 0 \tag{4}$$

For a tensile mooring line, such as the studied synthetic fiber rope here, it is regarded as a long slender tensile rod with negligible moments and shear forces, which can also experience large elongations. As a result, the bending stiffness B, the torsional stiffness H and the shear deformations can all be neglected in the above equations. Therefore, the only remaining internal force is caused by the cable tension tangential to the local direction. Finally, the governing equation is simplified as

$$(\lambda \mathbf{r}')' + \mathbf{q} = \rho\, \ddot{\mathbf{r}} \tag{5}$$

where λ is the Lagrange multiplier. The total external forces applied on a submerged slender rod per unit length are

$$\mathbf{q} = \mathbf{q}_{F-K} + \mathbf{q}_I + \mathbf{q}_D + \mathbf{q}_B + \mathbf{q}_G \tag{6}$$

where the first three terms represent the hydrodynamic forces, including Froude–Krylov force, $\mathbf{q}_{F-K}$, added mass force, $\mathbf{q}_I$, and drag force, $\mathbf{q}_D$; Li et al. [35] points out that damp models/forces are required to conduct the dynamic analyses of a structural system. Here, $\mathbf{q}_D$ stands for the damp forces, which are dependent on the velocities of the mooring line. It is noted that the fourth term, $\mathbf{q}_B$, is hydrostatic force; the last term, $\mathbf{q}_G$, is the gravity force. The total force $\mathbf{q}$ can be also expressed in detail as

$$\begin{aligned}\mathbf{q} = {} & \rho A(\mathbf{I} + C_{\mathrm{Mn}}\mathbf{N} + C_{\mathrm{Mt}}\mathbf{T})\mathbf{a} + \tfrac{1}{2}\rho D C_{\mathrm{Dn}}\mathbf{N}(\mathbf{v}-\dot{\mathbf{r}})\left|\mathbf{N}(\mathbf{v}-\dot{\mathbf{r}})\right| \\ & + \tfrac{1}{2}\rho D C_{\mathrm{Dt}}\mathbf{T}(\mathbf{v}-\dot{\mathbf{r}})|\mathbf{T}(\mathbf{v}-\dot{\mathbf{r}})| + \tfrac{(\rho A-\rho_t A_t)g\mathbf{e}_y}{(1+\epsilon)}\end{aligned} \tag{7}$$

where $\mathbf{T} = \mathbf{r'}^T\mathbf{r'}$ and $\mathbf{N} = \mathbf{I}-\mathbf{T}$, C_{Mn}, C_{Mt}, C_{Dn} and C_{Dt} are added mass coefficients in normal and tangential direction, drag coefficients in normal and tangential direction, respectively, while A_t, A and D denote the area of geometric cross section of the rod, the area of outer cross section of the rod and the diameter of the outer cross section of the rod. In the fluid domain, $\mathbf{v}$ and $\mathbf{a}$ represent velocity and acceleration of the ambient fluid, where the subscripts f, i and t denote the sea water, the fluid inside the tube and the tube itself.

At the same time, the dynamics of n tensile mooring line can be calculated in rectangular Cartesian coordinates. The governing equation and constraint equation for a tensile mooring line can be also expressed as

$$\frac{\partial(T\,\mathbf{t})}{\partial s} + \mathbf{q} = \rho\, \ddot{\mathbf{r}} \tag{8}$$

where T is the local tension, s is original length between one end to a waypoint along the rod, $\overline{S}$ is deformed length and $\mathbf{t}$ is the unit vector tangential to the deformed length expressed by $\mathbf{t} = \frac{\partial \mathbf{r}}{\partial s}$. The relation between deformed length and original length can be described as:

$$d\overline{s} = (1+\varepsilon)ds \tag{9}$$

$$\varepsilon = \frac{T}{EA} \tag{10}$$

where EA is the axial stiffness of the slender rod.

Therefore,

$$\mathbf{r}' = \frac{\partial \mathbf{r}}{\partial s} = \frac{\partial \mathbf{r}}{\partial \overline{s}}(1+\varepsilon) = \mathbf{t}(1+\varepsilon) \tag{11}$$

$$\mathbf{t} = \frac{\mathbf{r}'}{1+\varepsilon} \tag{12}$$

Substitute Equation (12) into Equation (8),

$$\left(\frac{T}{1+\varepsilon}\mathbf{r}'\right)' + \mathbf{q} = \rho\, \ddot{\mathbf{r}} \tag{13}$$

By comparing Equations (5) and (13), the Lagrange multiplier λ is defined as

$$\lambda = \frac{T}{1+\varepsilon} \tag{14}$$

Substitute Equation (14) into Equation (10),

$$\varepsilon = \frac{T}{EA} = \frac{\lambda}{EA-\lambda} = \frac{\frac{\lambda}{EA}}{1-\frac{\lambda}{EA}} = \frac{\bar{\varepsilon}}{1-\bar{\varepsilon}} \tag{15}$$

$$\bar{\varepsilon} = \frac{\lambda}{EA} \tag{16}$$

Additionally, **r** must satisfy a stretching constrain equation:

$$\mathbf{r}' \cdot \mathbf{r}' = (1+\varepsilon)^2 \tag{17}$$

By substituting Equation (15) into Equation (17),

$$\mathbf{r}' \cdot \mathbf{r}'(1-\bar{\varepsilon})^2 = 1 \tag{18}$$

2.2. Finite Element Simulation Approach

A global-coordinate-based nonlinear finite element method was used for the simplicity of numerical computation. The procedure for numerical implementation for the equations of motion in Equations (8) and (18) are the same as [36]. Galerkin's method was used to discretize the dynamic equations in space, resulting in a set of nonlinear 2nd-order ordinary differential equations in the time domain. Finally, a Newmark-β method was employed for time–domain integration of the discretized equations. For each element, the mooring line dynamic equation at the *K*th time step becomes:

$$\gamma_{ikm} M_{njm} \ddot{u}_{kj} + \beta_{ikm} \lambda_m u_{kn} = \mu_{im} q_{mn} + f_{in} \tag{19}$$

The coefficients in Equation (19) are obtained through integration over the length of the element:

$$\begin{array}{l} \beta_{ikm} = \frac{1}{L}\int_0^1 a_i'(\xi) a_k'(\xi) p_m(\xi) d\xi \\ \gamma_{ikm} = L\int_0^1 a_i(\xi) a_k(\xi) p_m(\xi) d\xi \\ \mu_{im} = L\int_0^1 a_i(\xi) p_m(\xi) d\xi \end{array} \tag{20}$$

Similarly, the constrain equation is discretized as

$$\beta_{ikm} u_{in} u_{kn} + \eta_{iklm}(-2\bar{\varepsilon}_l + \bar{\varepsilon}_l^2) u_{in} u_{kn} - \tau_m = 0 \tag{21}$$

The coefficients in Equation (21) are obtained through integration over the length of the element:

$$\begin{array}{l} \tau_m = L\int_0^1 p_m(\xi) d\xi \\ \eta_{iklm} = \frac{1}{L}\int_0^1 a_i'(\xi) a_k'(\xi) p_l(m) p_m(\xi) d\xi \end{array} \tag{22}$$

where $a(s)$ is the Hermite cubic shape function, and $p(s)$ is the quadratic shape function, ξ is a nondimensional position expressed as $\xi = s/L$, L is the original length of the element.

During simulations, the tensile mooring line was discretized into 100 line elements each, which should be solved as per the relation expressions in Equations (19) and (21) using Newmark-β method. The boundary conditions for the finite element simulations of the mooring lines include the first element that was attached to the fairlead of the floating wind turbine while the 100th element was connected to the seabed. So, the first element transferred the pretension force to the wind turbine and, in turn, moved following the motion of the wind turbine. The last element was treated to be fixed at the seabed. To begin with the dynamic analysis of the mooring lines, static analysis was conducted to achieve the static equilibrium position, namely, the initial condition for mooring dynamic analysis.

The time step was set as 0.05 s to achieve independence while the whole simulation time lasted 30 wave excitation time cycles. After the simulation was finished, 15 total unknowns relating to u and λ were obtained.

2.3. Dynamics of the Spar-Type Floating Wind Turbine

Hydrodynamic forces applied on the body can be computed by nonlinear diffraction/radiation theory or the Morison equation. Since the diameter of the foundation was very small compared with the wave length, the foundation was considered as a hydro-transparent structure, and thus the Morison equation was used to calculate the hydrodynamic forces acting on the foundation as follows:

$$\widetilde{\mathbf{F}}_{Morison} = \mathbf{F}_L(\mathbf{a}, \mathbf{a}_b) + \mathbf{F}_{NL}(\mathbf{v}, \mathbf{v}_b, \mathbf{v}_c) \tag{23}$$

where the first term, $\mathbf{F}_L(\mathbf{a}, \mathbf{a}_b)$ is linear term (inertial forces) and the other term, $\mathbf{F}_{NL}(\mathbf{v}, \mathbf{v}_b, \mathbf{v}_c)$ is nonlinear (viscous-drag) term in Morison's equation; $\mathbf{a}_b$ and $\mathbf{v}_b$ are the acceleration and velocity of the foundation, respectively, $\mathbf{v}_c$ is the velocity of the current. Due to the variations in the horizontal components of the water particle velocities with the submerged depth induced by wave and current, the inertial forces and viscous-drag forces in Morison's equation were discretized into N segments along the submerged length. Correspondingly, the hydrodynamics forces can be expressed as:

$$\mathbf{F}_L(\mathbf{a}, \mathbf{a}_b) = \sum_{q=1}^{N} d\mathbf{F}_{L,q}(\mathbf{a}_q, \mathbf{a}_b) dL_q \tag{24}$$

$$\mathbf{F}_{NL}(\mathbf{v}, \mathbf{v}_b, \mathbf{v}_c) = \sum_{q=1}^{N} d\mathbf{F}_{NL,q}(\mathbf{v}_q, \mathbf{v}_b, \mathbf{v}_{c,q}) dL_q \tag{25}$$

With the hydrodynamic forces per unit of length of the foundation shown as:

$$d\mathbf{F}_{L,q}(\mathbf{a}_q, \mathbf{a}_b) = (1 + C_a)\rho \frac{\pi {D_q}^2}{4} \mathbf{a}_q - C_a \rho \frac{\pi {D_q}^2}{4} \mathbf{a}_b \tag{26}$$

$$d\mathbf{F}_{NL,q}(\mathbf{v}_q, \mathbf{v}_b, \mathbf{v}_{c,q}) = \frac{1}{2} C_d \rho C D_q \left| \mathbf{v}_q + \mathbf{v}_{c,q} - \mathbf{v}_b \right| (\mathbf{v}_q + \mathbf{v}_{c,q} - \mathbf{v}_b) \tag{27}$$

where dL_q is the length of qth segment, the subscript q denotes the qth section, D_q is the diameter of qth segment of the foundation, C_a and C_d refer to the added mass and drag coefficients, respectively. The discretized forces were integrated over the whole length of the foundation, L.

2.4. Coupling Dynamics of the Spar-Type Floating Wind Turbine with Taut Mooring System

Similar to other floating devices or platforms, such as wave energy converter, tidal converter, etc., nonlinear dynamic analysis is the most reliable approach for estimating the vulnerability subjected to different external pulses [37]. To accomplish the coupling dynamic analysis of a floating wind turbine foundation with mooring system, as shown in Figure 3, the equations of motion for the foundation shown in Equations (28) and (29) and mooring lines shown in Equations (5) and (18) were solved simultaneously using Newmark-β method. The six degree-of-freedom (6 DOF) nonlinear motion equations of a rigid body were derived as follows [38–41]:

$$m\ddot{\tilde{\xi}} + m\mathbf{T}^t(\dot{\boldsymbol{\omega}} \times \mathbf{r}_g) + m\mathbf{T}^t(\boldsymbol{\omega} \times (\boldsymbol{\omega} \times \mathbf{r}_g)) = \widetilde{\mathbf{F}} \tag{28}$$

$$\mathbf{I}\dot{\boldsymbol{\omega}} + \boldsymbol{\omega} \times \mathbf{I}\boldsymbol{\omega} + m\mathbf{r}_g \times \left(\mathbf{T}\ddot{\tilde{\xi}}\right) = \mathbf{M} \tag{29}$$

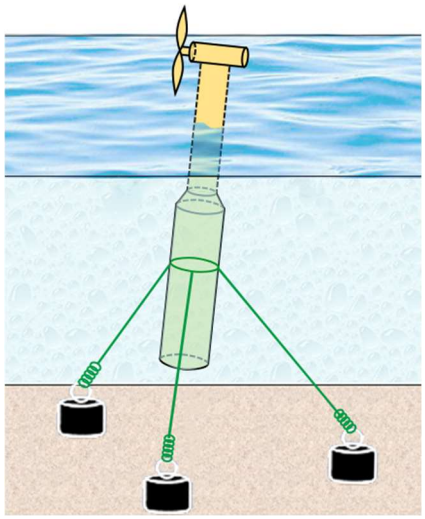

Figure 3. Spar-typed wind turbine with its taut mooring lines.

The translational motion and the rotational motion of a rigid body are expressed in the spaced-fixed coordinate system $OXYZ$ with origin at O and the body-fixed coordinate system $oxyz$ with origin at o, respectively. Where ξ is the translational displacement of the body at point o in $OXYZ$, $\boldsymbol{\omega}$ is the rotational velocity in $OXYZ$; $\mathbf{r}_g = (x_g, y_g, z_g)^t$; is the point vector of mass center of the body in $OXYZ$; $\mathbf{I}$ is the moment of inertia of the body, with respect to point o in $OXYZ$; $\mathbf{T}$ is a transfer matrix between the $oxyz$ and $OXYZ$. Given the total external forces $\widetilde{\mathbf{F}}$ acting on the body in $OXYZ$ and the total external moments with respect to o, $\mathbf{M}$ can be unified by $\mathbf{F}$, as shown in

$$\mathbf{F} = \begin{bmatrix} \widetilde{\mathbf{F}} \\ \mathbf{M} \end{bmatrix} \tag{30}$$

Correspondingly, the 6 DOF motion equations for the floating foundation can be derived as

$$[\mathbf{M}_b + \mathbf{M}_a]\ddot{\mathbf{X}}(t) + \mathbf{C}\mathbf{X}(t) = \mathbf{F}_H + \mathbf{F}_{Morison} + \mathbf{F}_M + \mathbf{F}_\varepsilon \tag{31}$$

$$\mathbf{F}_e = \left\{ \begin{array}{l} -m\mathbf{T}^t(\boldsymbol{\omega} \times (\boldsymbol{\omega} \times \mathbf{r}_g)) - m\mathbf{T}^t(\boldsymbol{\alpha}_q \times \mathbf{r}_g) \\ -\boldsymbol{\omega} \times \mathbf{I}_o\boldsymbol{\omega} - \mathbf{I}_o\boldsymbol{\alpha}_q \end{array} \right\} \tag{32}$$

where $\mathbf{M}_b$ and $\mathbf{M}_a$ are the mass and added mass of the foundation, respectively, $\mathbf{C}$ is the hydrostatic stiffness matrix, $\mathbf{F}_H$ represent nonlinear hydrostatic restoring forces, $\mathbf{F}_{Morison}$ denotes Morison forces, and $\mathbf{F}_M$ refers to mooring line forces. The generalized form of Equation (31) can be expressed as

$$\mathbf{A}\ddot{\mathbf{X}}(t) + \mathbf{C}\mathbf{X}(t) = \mathbf{F}(t) + \mathbf{F}_M(t) \tag{33}$$

where $\mathbf{F}_M(t)$ denotes mooring line forces and $\mathbf{F}(t)$ denotes the rest of forces. At the Kth time step, the motion equation can be re-written in the following form

$$\mathbf{A}^{(K)}\ddot{\mathbf{X}}(t)^{(K)} + \mathbf{C}^{(K)}\mathbf{X}^{(K)} = \mathbf{F}^{(K)} + \mathbf{F}_M{}^{(K)} \tag{34}$$

Correspondingly, a numerical modelling code, which is composed of a main program and a subroutine program, was developed based on the existing code Cable3D proposed by [33]. The subroutine program, namely a mooring dynamics program developed according to Section 2.1, was called by the main program at each time step to calculate the motions of the foundation. It should be noted that the values of f_{in} in Equation (19) were transmitted to $\mathbf{F}_M{}^{(K)}$ in Equation (34) through the hinged boundary conditions.

3. Comparative Study between Stiff and Tensile Mooring Lines

The developed model has been applied into the analyses of the dynamic responses of a spar-type floating wind turbine foundation moored by taut mooring system. The calculated results in terms of dynamic responses of the foundation and the mooring tensions are compared by using the traditional stiff mooring line proposed by [33,36] and the new tensile mooring line model proposed in this paper, respectively.

3.1. Model Geometry and Mooring Configuration

The spar-type floating wind turbine foundation studied in the research is a small vertical cylinder with its mass uniformly distributed. The main particulars of the foundation are given in Table 1. The foundation is moored by three taut mooring lines, namely a three-point mooring system (T3), as shown in Figure 4a. The configuration details for the mooring system are listed in Figure 4b and Table 2. The fairlead points of each mooring line are at the same elevation as the gravity center of the foundation. Detailed geometric and physical properties of the mooring lines are shown in Table 3.

Table 1. Main particulars of the foundation.

Parameters	Value	Unit
Max Diameter	3.00	m
Draft	1.00	m
Height	2.00	m
Weight	7245.0	KG
Rx (gyration radius)	0.90	m
Rx	0.90	m
Rz	1.10	m

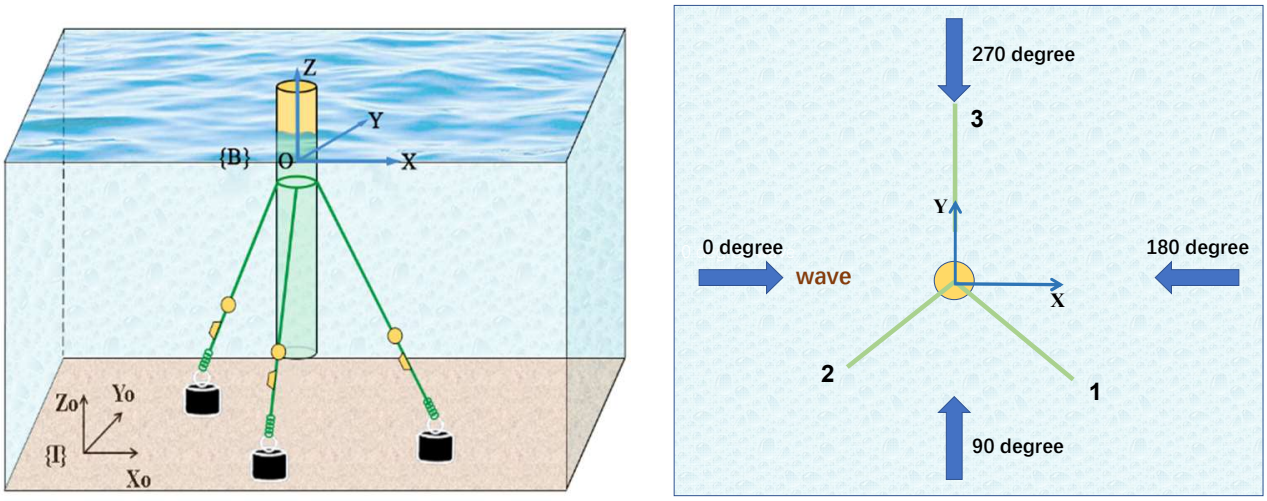

Figure 4. Foundation with its three-point taut mooring system (T3). (**a**) 3D view, (**b**) top view.

Table 2. Properties of mooring system.

Type	Pretension (KN)	Arrangement (Degree)	Length (m)
T3	36.00	90/210/330	100.00

Table 3. Properties of mooring lines.

Parameters	Value	Unit
Composition	Polyester	-
Diameter	32.0	mm
Unit Wet Weight	0.000622	tone
EA	17,789.13043	KN
Breaking Strength	818.3	KN

3.2. Results and Analysis

The floating wind turbine foundation coupled with a T3 mooring system is simulated by using the developed code Cable3D, according to the proposed methodology. The developed code Cable3D has been validated in Xiang [37] by comparing the simulated data with corresponding data measured from wave basin test. The simulations are performed using a regular wave with a wave height of 1.2 m, a period of 5 s, wave heading of 0 degree and water depth at 45 m. Figure 4 shows the comparison of surge and heave motions using the traditional stiff mooring line model and tensile mooring line model proposed in this paper, respectively. Through the comparisons, it is found that that the surge and heave motions of the foundation using traditional stiff mooring line model will underestimate the range of the motion responses of the foundation. In real situations, the elongation of the mooring line cannot be ignored, since the elongation of the mooring line will make the whole floating wind turbine system less stiff and more elastic. Figure 5 shows the comparison of corresponding tension forces at the fairlead of three mooring lines. It can be found that tensions at Line 1 and Line 2 calculated by stiff mooring line model are much larger than stiff mooring line model. This is because the surge motion of the foundation is larger in the tensile mooring line model than in the stiff mooring line model; much larger tension forces at the fairlead of mooring line 1 and 2 whose configurations are more aligned with surge direction are required to limit the surge responses of the foundation. Additionally, it is noted that, as shown in Table 3, the mooring line is made of polyester, which in reality can hardly be compressed. However, in Figure 5, it is observed that when using the traditional mooring line model, the calculated minimum mooring tension force of line 3 is much smaller than zero, which means the mooring line can be compressed a lot during wave-induced dynamic motions. By ignoring the bending stiffness of the mooring line, the proposed tensile mooring line model can overcome the inaccuracy of predicting the compressions of the elastic mooring line, such as polyester using traditional stiff mooring line model.

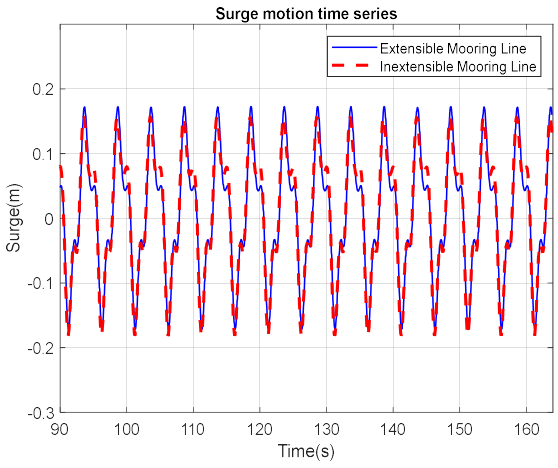

(**a**)

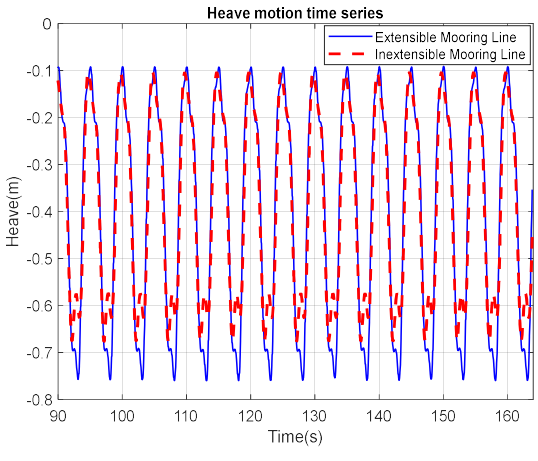

(**b**)

Figure 5. *Cont.*

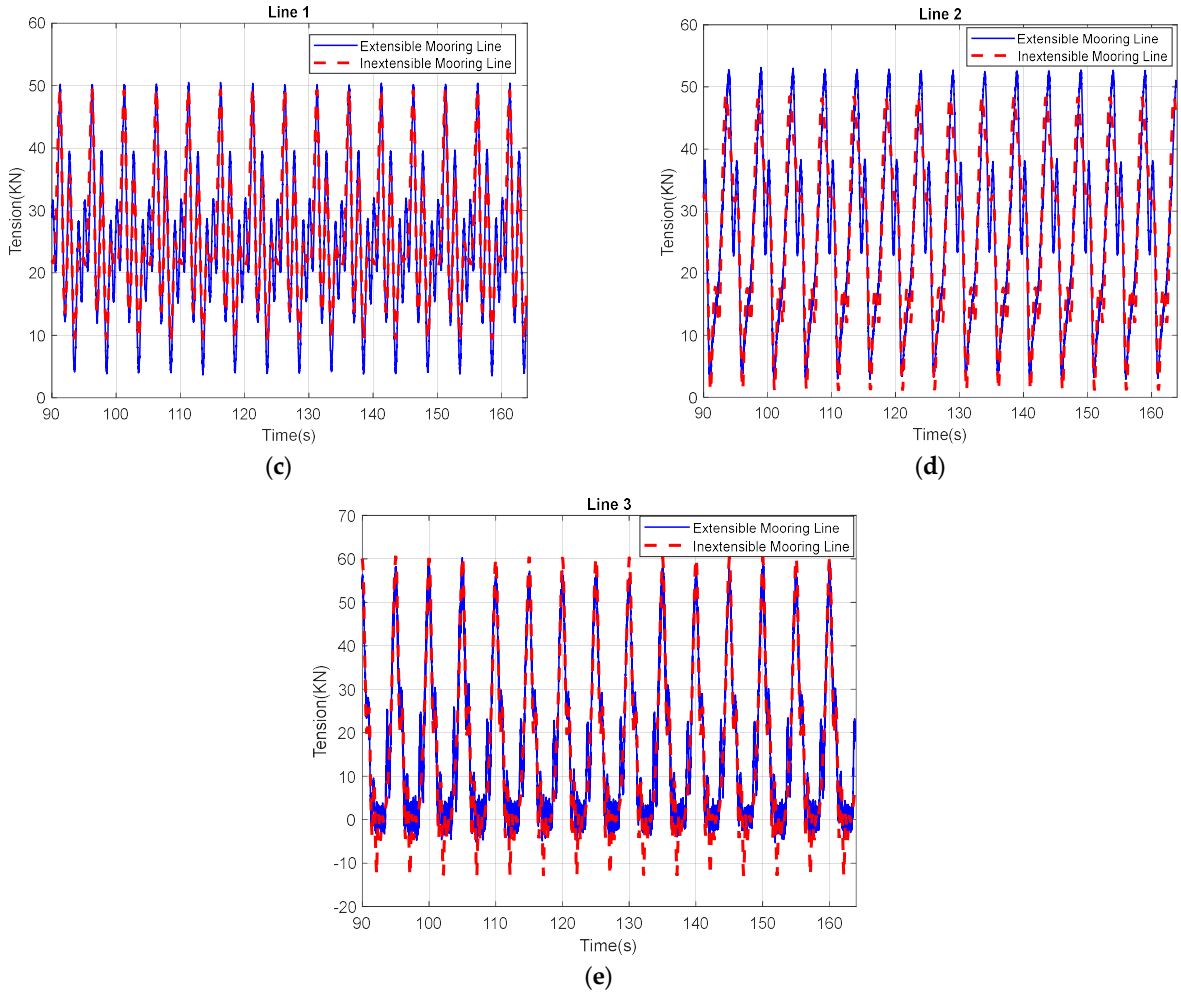

Figure 5. Comparison of time series of surge and heave motion time series, mooring tension at the fairlead using traditional stiff line model and proposed tensile mooring line model, (**a**) Surge (**b**) Heave (**c**) Line 1 (**d**) Line 2 (**e**) Line 3.

4. Sensitivity Study and Analysis

The developed numerical code is utilized for studying the same foundation but with a shallower initial draft, 1.0 m and under higher regular waves and H = 2 m, compared with the case in Section 3. The material properties of the mooring lines are the same as those shown in Table 3. Multiple simulation cases are conducted as shown in Table 4. Firstly, Case1–Case3 study a T3 mooring system with variations in mooring length; Case1, Case4 and Case5 study the T3 mooring system with variations in pretension force. Next, two different taut mooring systems: two-point (T2) and three-point (T3) system are investigated. Three representative wave headings at 0, 45 and 90 degrees are simulated for T2, which correspond to Case 9–Case 11, and 30, 60 and 90 degrees for T3, which correspond to Case 6–Case 8.

4.1. Effect of Mooring length

The static test for a single mooring line is simulated for Case1–Case3, corresponding to the length of the mooring lines increasing from 75 m to 80 m and 85 m (Figure 6). Before static test, the zero horizontal offset location is defined when the foundation and associated T3 mooring systems are completely static, as shown in Figure 4a. In the static simulation test, one single mooring line is picked and kept from the static T3 mooring system while the other two mooring lines are removed. The fairlead point of the mooring line moves with the variation in horizontal offset: −1.0 m to 1.0 m. The anchor point of each single

mooring line is determined according to the initial settings for the whole mooring system in Table 4. After simulations, the comparisons of the stiffness curve of a single mooring line with different lengths are presented in Figure 7a. It can be found that although the shorter mooring line has smaller mooring tension at horizontal offset = 0 m, its stiffness is larger than longer mooring lines, resulting in larger mooring tension when the horizontal offset exceeds 0.3 m.

Table 4. Properties of mooring system.

Case	Type	Pretension (P)	Arrangement (Line 1/2··)	Length	Wave Heading
		(KN)	(degree)	(m)	(degree)
1	T3	57.00	90/210/330	75.00	0
2	T3	57.00	90/210/330	80.00	0
3	T3	57.00	90/210/330	85.00	0
4	T3	47.00	90/210/330	75.00	0
5	T3	52.00	90/210/330	75.00	0
6	T3	57.00	90/210/330	75.00	30
7	T3	57.00	90/210/330	75.00	60
8	T3	57.00	90/210/330	75.00	90
9	T2	62.00	0/180	75.00	0
10	T2	62.00	0/180	75.00	45
11	T2	62.00	0/180	75.00	90

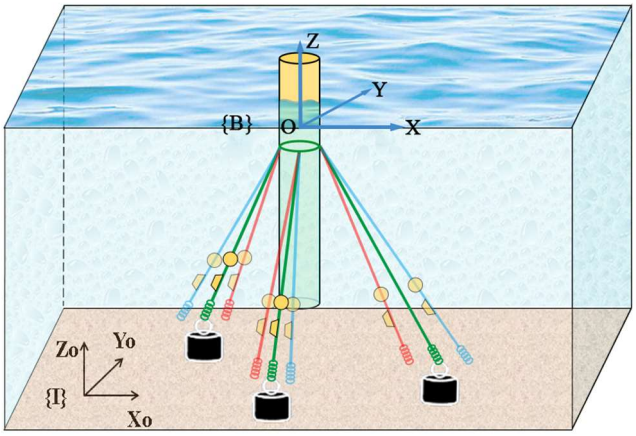

Figure 6. Mooring configuration with different lengths at L1 = 75 m, L2 = 80 m and L3 = 85 m.

The dynamic simulations of a foundation with three mooring lines are carried out by varying the length of each mooring line from L1 = 75 m to L2 = 80 m and L3 = 85 m, as shown in Figure 6. The dynamic responses of the foundation with time are presented in Figures 7b and 8. Figure 7b shows motion time series in the X-Y plane, a surge of the foundation with a variation in mooring length. The surge motions at mooring length of 75 m is much larger than 80 m and 85 m. This may be because the mooring tension at the mooring length of 75 m is relatively smaller before reaching a certain distance, as shown in Figure 7a. A relatively large heave motion will be allowed. Figure 8 shows out-of-plane heave and pitch motion time series of the foundation with variations in mooring length. The heave displacement in a downward direction at mooring length of 75 m is much larger than mooring length of 80 m and 85 m. This is because for a smaller mooring length of 75 m, the angle between the mooring line and the vertical axis of the foundation is relatively small. As a result, the vertical component of the mooring tension at the fairlead point will be the largest, which will pull the floating foundation further into the water. Thus, the

balance position of heave motions of the foundation at a mooring length of 75 m will be lower than the others. Similar findings can be found in the statistical data for all the 6 DOF motions of the foundation, as provided in Table 5. It is found that the largest maximum value and mean value for the 6 DOF motion amplitudes of the foundation all occurred at mooring lengths of 75 m, compared to 80 m and 85 m.

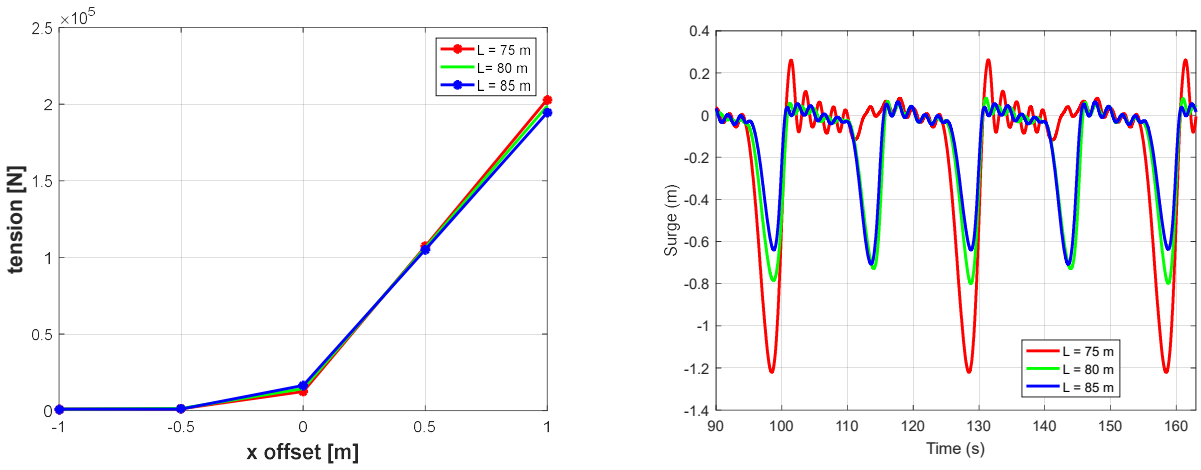

(**a**) (**b**)

Figure 7. In-plane motions with variations in mooring length. (**a**) stiffness curve, (**b**) surge time series.

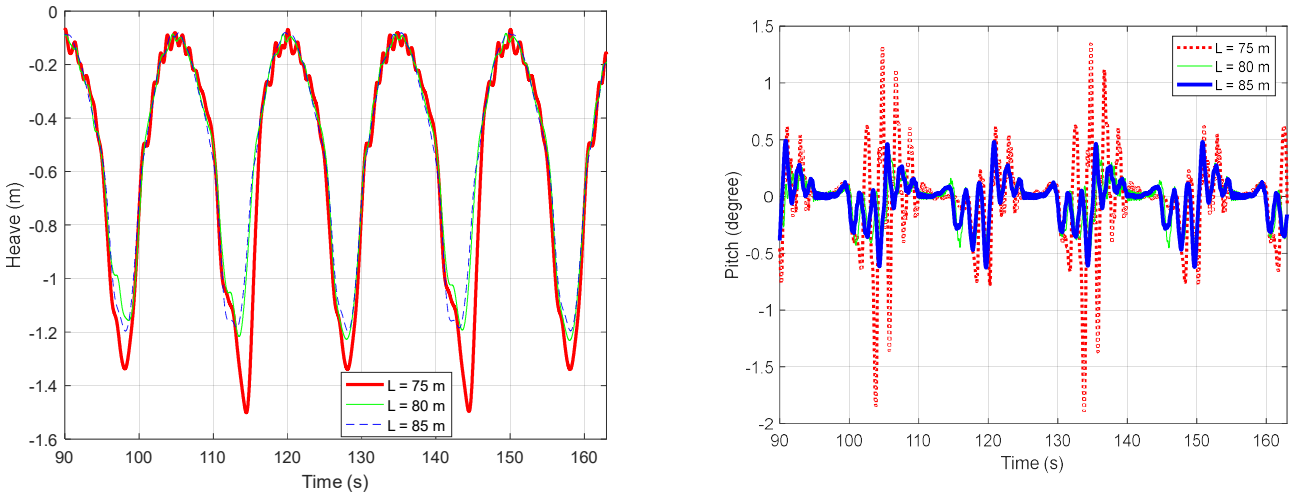

(**a**) (**b**)

Figure 8. Out-of-plane motions with variations in mooring length. (**a**) heave time series (**b**) pitch time series.

The mooring load is another critical consideration for evaluating the performance of the mooring system. The mooring line at the fairlead usually suffers the largest loads; thus, the time series of mooring tension at the fairlead are studied and plotted in Figure 9 for each mooring line. The statistical data: maximum value and mean value for the time domain mooring loadings at the fairlead are displayed in Table 6. It can be found that Line1 at L1 = 75 m experiences the largest mooring load, 71.46 KN. There are four (the most) largest amplitude values (maximum value for line 1 and line 2, mean value for line 1 and line 2) occurring at L1 = 75 m. This is because when L1 = 75 m, the displacement of the 6 DOF of the foundation is largest and the stiffness of the mooring line at L1 = 75 m is also largest, as shown in Figure 7a.

Table 5. Comparison of 6 DOF motions of foundations with different mooring lengths.

Parameter	L = 75 m		L = 80 m		L = 85 m	
	Max	Mean	Max	Mean	Max	Mean
Surge (m)	1.22	0.15	0.87	0.13	0.71	0.12
Sway (m)	2.87	0.49	1.32	0.29	0.95	0.23
Heave (m)	1.66	0.53	1.23	0.49	1.21	0.50
Roll (deg)	47.50	11.90	40.30	9.12	29.17	7.91
Pitch (deg)	1.89	0.19	0.92	0.13	0.63	0.12
Yaw (deg)	8.48	1.82	8.39	1.24	3.86	0.87

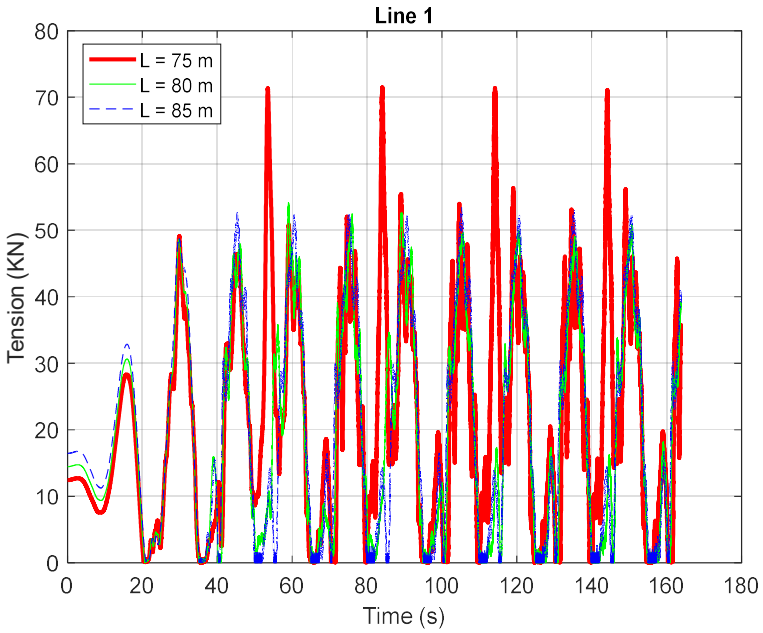

(**a**)

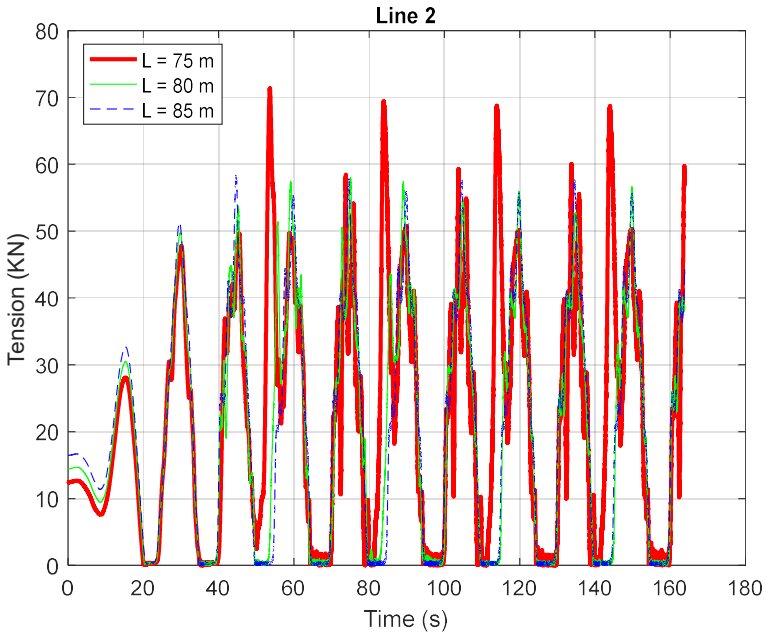

(**b**)

Figure 9. *Cont.*

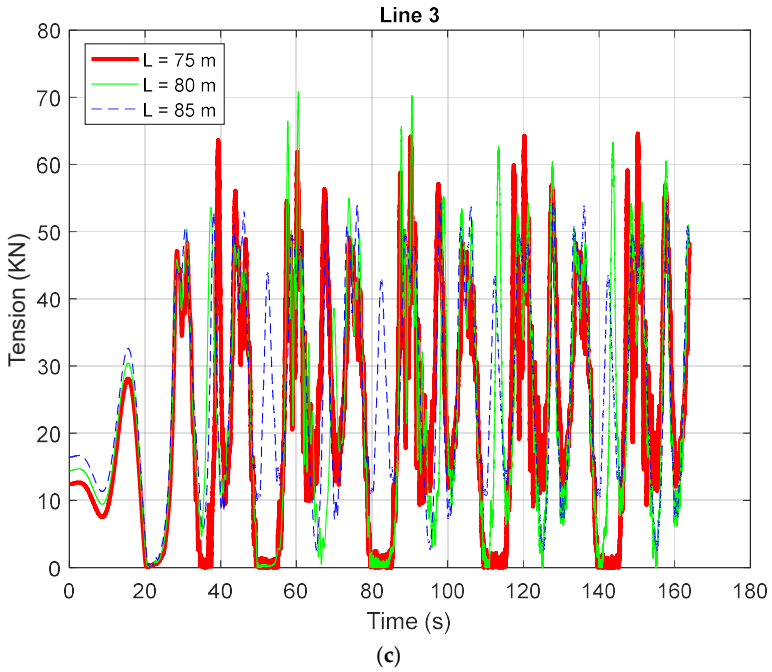

(**c**)

Figure 9. Time series of mooring tension at the fairlead with variations in mooring length, (**a**) Line 1, (**b**) Line 2, (**c**) Line 3.

Table 6. Comparison of mooring tensions at the fairleads of foundations with different mooring lengths.

Parameter	L = 75 m	L = 80 m	L = 85 m
Max-Line 1 (KN)	71.46	54.18	53.66
Max-Line 2 (KN)	71.35	58.04	58.34
Max-Line 3 (KN)	64.58	70.84	54.54
Mean-Line 1 (KN)	21.54	19.66	20.33
Mean-Line 2 (KN)	21.87	19.96	20.42
Mean-Line 3 (KN)	22.07	23.14	26.15

4.2. Effect of Pretension

Case 4–6 display the simulation procedures of the same foundation with a fixed mooring length but different pretension forces. Figure 10a shows comparisons of the stiffness curve of a single mooring line with different pretensions. It can be found that the mooring line with smaller pretension has smaller mooring tension at a horizontal offset of 0 m; the stiffness of the shorter mooring line stays the same with variations in the pretension. The results of the three case studies are compared in Figures 10b and 11. The results from the simulation of Figures 10b and 11 show that by increasing the pretension of the mooring line, the amplitude of surge and heave do not get affected significantly, but the pitch decreased apparently.

The statistical data: Maximum value and mean value for the foundation time domain motion responses are reported in Table 7. It is found that the maximum and mean values for Case 4–6 are very close. Almost all the largest maximum values and mean values occur at pretension force, P = 47 KN.

The mooring tension time series are plotted in Figure 12 for line 1, line2 and line3, respectively. The statistical data: maximum value and mean value for the time domain mooring loadings at the fairlead are displayed in Table 8. It can be found that the largest mooring loads is 76.08 KN, happening at line 2 with P = 47 KN. There are four (the most) largest amplitude values (maximum value for line 3; mean value for line 1, line 2 and line

3) occurring at P = 57 KN. This may be because the mooring tension at P = 57 KN in static test is the largest at the same offset in Figure 10a, although the displacement is very close, as shown in Table 8.

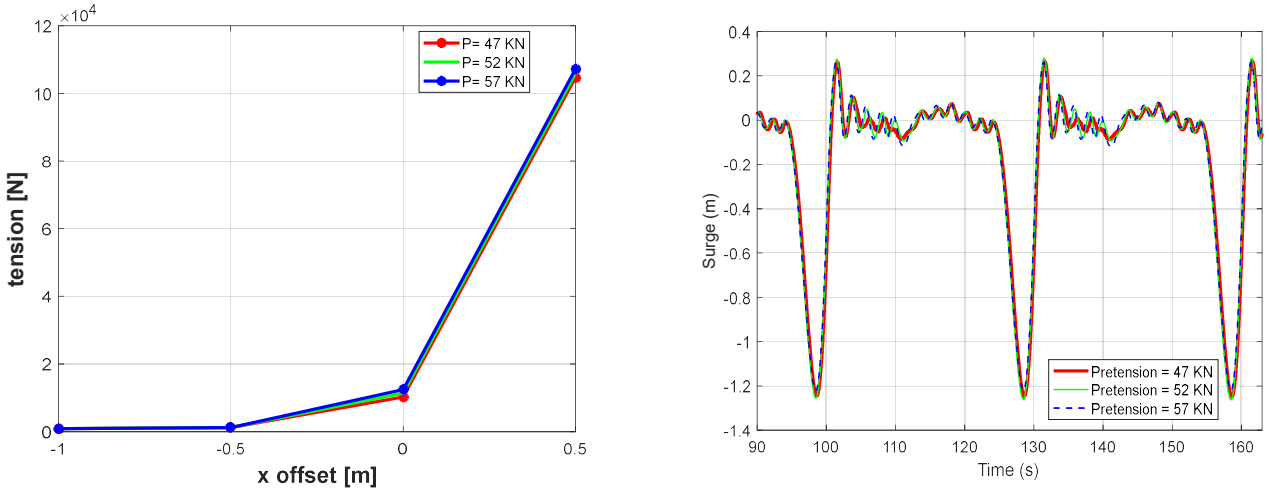

Figure 10. In-plane motions with variations in pretension. (**a**) Stiffness curve, (**b**) surge time series.

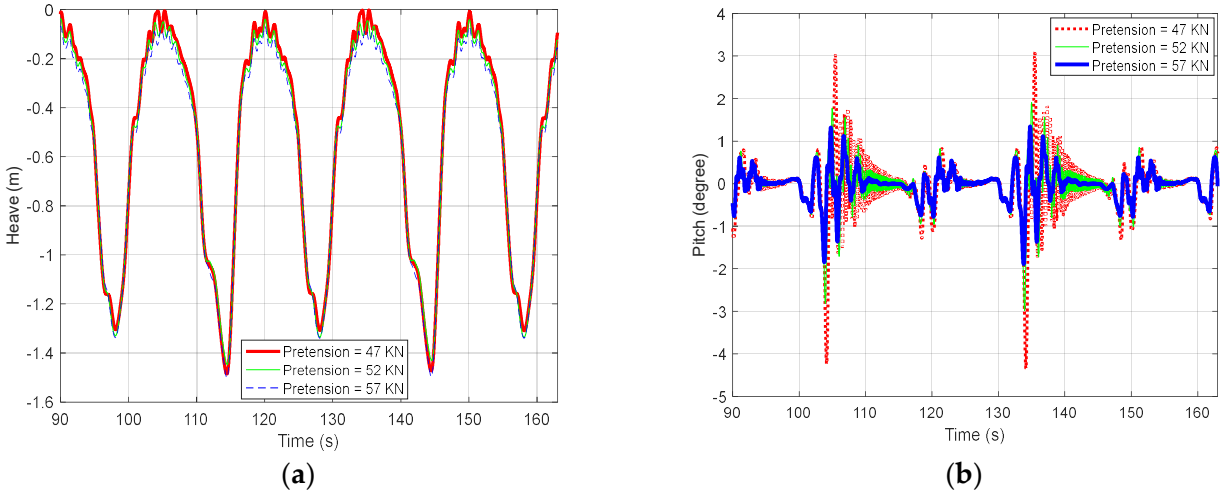

Figure 11. Out-of-plane motions with variations in pretension. (**a**) Heave time series, (**b**) pitch time series.

Table 7. Comparison of 6 DOF motions of foundations with different pretension loads.

Parameter	P = 47 KN		P = 52 KN		P = 57 KN	
	Max	Mean	Max	Mean	Max	Mean
Surge (m)	1.25	0.15	1.25	0.15	1.22	0.15
Sway (m)	3.06	0.52	3.00	0.51	2.87	0.49
Heave (m)	1.75	0.49	1.74	0.51	1.66	0.53
Roll (deg)	48.53	12.30	48.21	12.14	47.51	11.93
Pitch (deg)	4.34	0.32	2.97	0.24	1.89	0.19
Yaw (deg)	10.86	2.04	9.42	1.94	8.48	1.82

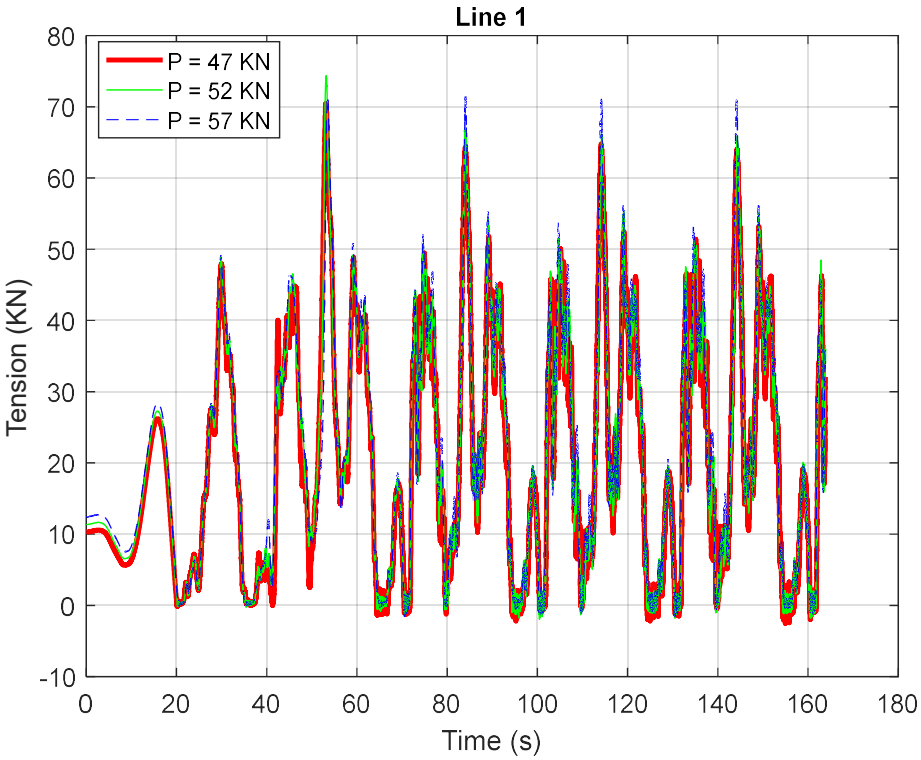

(**a**)

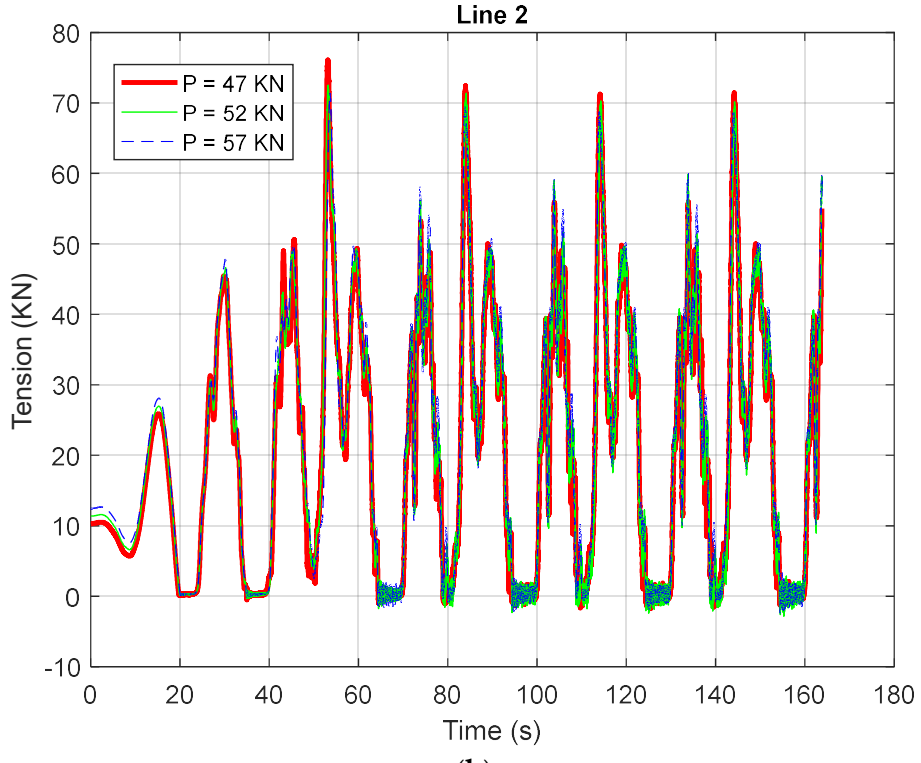

(**b**)

Figure 12. *Cont.*

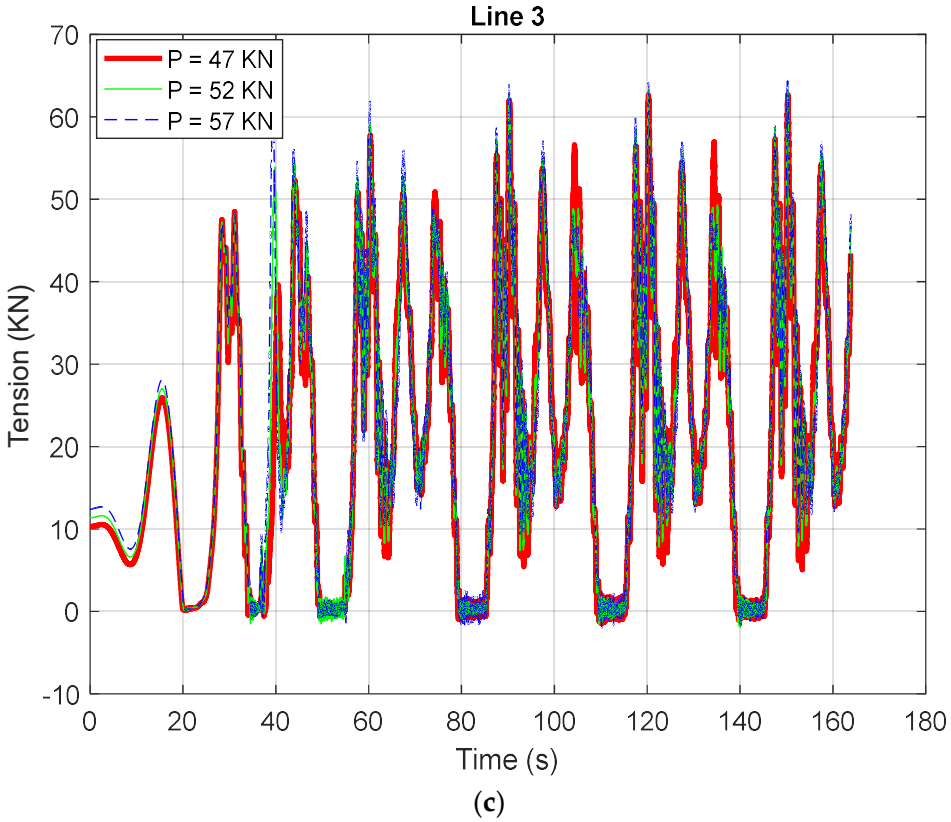

Figure 12. Time series of mooring tension at the fairlead with variations in pretension, (**a**) Line 1 (**b**) Line 2, (**c**) Line 3.

Table 8. Comparison of mooring tensions at the fairleads of foundations with different pretension loads.

Parameter	P = 47 KN	P = 52 KN	P = 57 KN
Max-Line 1 (KN)	70.46	74.35	71.46
Max-Line 2 (KN)	76.08	72.49	71.35
Max-Line 3 (KN)	62.72	63.14	64.58
Mean-Line 1 (KN)	20.36	20.89	21.54
Mean-Line 2 (KN)	20.62	21.21	21.87
Mean-Line 3 (KN)	20.82	21.49	22.07

4.3. Effect of Number of Mooring Lines

Two taut mooring systems: T2 with two mooring lines and T3 with three mooring lines are studied in this section. In order to study the dynamic responses of the foundation under different unidirectional wave cases, simulations for wave headings from 0–360 degrees are supposed to be conducted. However, considering the geometric symmetric characteristics of each mooring system, with reference to the coordinate system, T2 wave headings at 0–90 degrees and T3 wave headings at 30–90 degrees will be able to cover all the unidirectional waves. To reduce the simulation time, only three typical wave headings are considered for each mooring system: 0, 45 and 90 degrees for T2 (Case 9–11) and 30, 60 and 90 degrees for T3 (Case 6–8).

Further statistical analysis on the motion response data accumulated from Case 7–9 for T3 and Case 10–12 from T2 allows for an overall evaluation of the dynamic responses of the foundation. Since T2 and T3 have different configuration with respect to the coordinate system, a comparison of total in-plane displacement, $R = \sqrt{X^2 + Y^2}$, as indicated by *OP* in

Figure 13, between T2 and T3 is more appropriate and reasonable instead of comparing their X and Y coordinates. Figure 14a presents the histogram of R for T2 and T3. It can be found that for T2 and T3, the ranges of R both vary from 0–2.5 m. T3 occurs more than T2 when R is less than about 0.75 m and less than T2 when R is larger than 0.75 m. The motion responses of the foundation with T3 are smaller than T2 in the X-Y plane, since the displacement of the foundation focuses on the lower end values of the range for T3 but the upper end values for T2. The out-of-plane displacement Z is represented by *PO′* in Figure 13. The histogram of the out-of-plane displacement Z for T2 and T3 are compared in Figure 14b. The range of the out-of-plane displacement for T2 and T3 vary from 0–0.8 m and 0–1.2 m, respectively. T3 occurs more than T2 when the out-of-plane displacement is less than 0.2 m, less than T2 when the displacement is more than 0.2 m and less than 0.8 m, and again more than T2 when the displacement is more than 0.8 m. The out-of-plane motion responses of the foundation with T2 are more stable than T3, since the out-of-plane displacement of the foundation concentrates on the middle values of the range for T2 but on two ends (lower end and upper end) for T3.

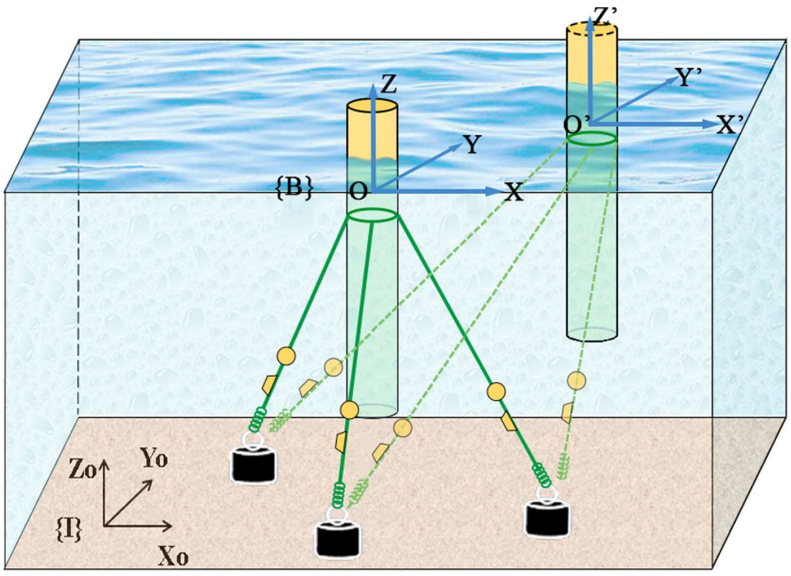

Figure 13. The in-plane and out-of-plane displacement of a foundation under waves.

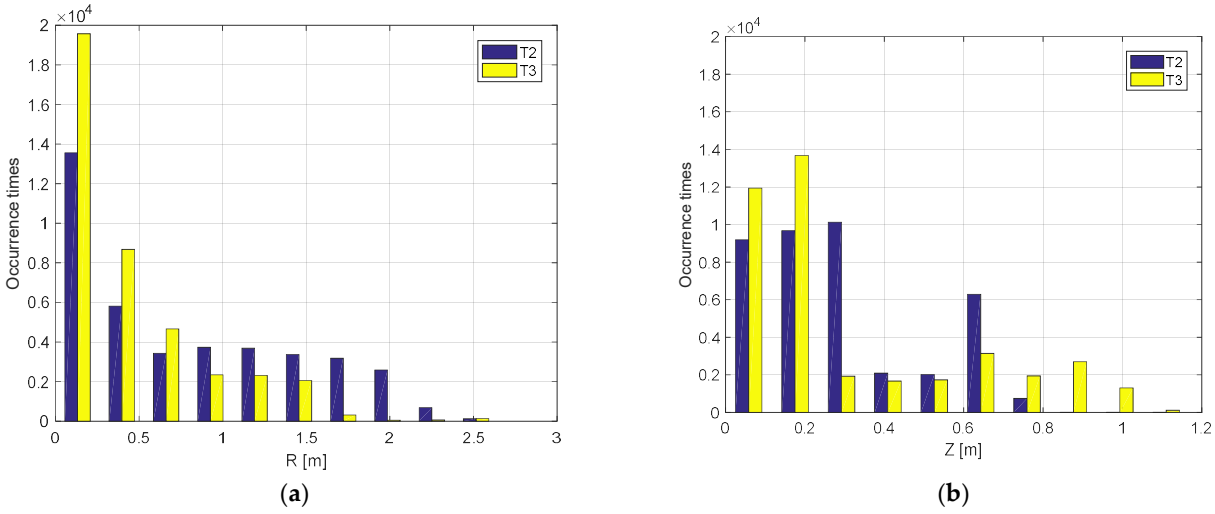

Figure 14. Histogram comparison of the displacement of foundation with T2 and T3. (**a**) In-plane displacement, (**b**) out-of-plane displacement.

5. Conclusions

In this paper, a finite element based tensile mooring line model is developed to study the statics and dynamics of mooring lines experiencing large elongations, such as synthetic fiber mooring lines. A developed time domain modelling code is applied to studying the dynamics of a floating foundation. The main contributions of the present paper include:

1. A new approach based on the tensile mooring line model is particularly proposed for the dynamic response analysis of the floating wind turbine foundation, coupled with a taut mooring system. The comparison of simulated results in terms of mooring tension and motion response of the wind turbine foundation using a traditional stiff mooring model and tensile mooring line model, respectively, demonstrates the much higher accuracy of the proposed tensile mooring line model when predicting the dynamic responses of the foundation and taut mooring tensions.
2. Design parameters, such as the length and pretension of the mooring lines, are found to have a significant influence on the dynamic responses of the floating wind turbine foundation. The largest maximum value and mean value for each of the 6 DOF motion responses of the foundation all occur at a relatively small mooring length, resulting in the occurrence of the largest amplitude values of mooring tension at the fairleads for Line1, Line2, and Line3. The largest maximum values and mean values of the motion responses of the foundation almost all happen at a relatively small pretension force, but the largest amplitude values of the mooring loads at the fairlead occur at a large pretension force.
3. A thorough comparative performance analysis of the foundation connected with two different mooring configurations, two-point (T2) and three-point (T3) taut mooring systems, are studied via the proposed method. The comparisons of simulation results between two different mooring configurations displayed: the motion responses of the foundation with T2 are larger than T3 in the X-Y plane, but the out-of-plane motion responses of the foundation with T2 are more stable than T3.

Author Contributions: Conceptualization, G.X., X.X. and X.Y.; methodology, G.X. and X.Y.; software, G.X. and X.Y.; investigation, G.X. and X.X.; resources, G.X. and X.X.; writing—original draft preparation, G.X.; writing—review and editing, G.X. and X.X. All authors have read and agreed to the published version of the manuscript.

Funding: This work is supported by National Natural Science Foundation of China, grant number 5213000376 and Hubei Provincial Natural Science Foundation for Innovation Groups, grant number 2021CFA026, in part by the Fundamental Research Funds for the Central Universities, grant number 2021XJJS016.

Institutional Review Board Statement: Not applicable.

Informed Consent Statement: Not applicable.

Data Availability Statement: Not applicable.

Conflicts of Interest: The authors declare no conflict of interest.

References

1. Fitzgerald, J.; Lars, B. Including Moorings in the Assessment of a Generic Offshore Wave Energy Converter: A Frequency Domain Approach. *Mar. Struct.* **2008**, *21*, 23–46. [CrossRef]
2. Kim, J.D.; Jiang, B.S. Application of multi-objective optimization for TLP considering hull-form and tendon system. *Ocean. Eng.* **2016**, *116*, 142–156. [CrossRef]
3. Ahmed, F.; Xiang, X.B.; Jiang, C.C.; Xiang, G.; Yang, S.L. Survey on traditional and AI based estimation techniques for hydrodynamic coefficients of autonomous underwater vehicle. *Ocean. Eng.* 2023. [CrossRef]
4. Sergiienko, N.Y.; Rafiee, A.; Cazzolato, B.S.; Ding, B.; Arjomandi, M. A feasibility study of the three-tether axisymmetric wave energy converter. *Ocean. Eng.* **2018**, *150*, 221–233. [CrossRef]
5. Wang, Z.; Yang, S.L.; Xiang, X.B.; Vasilijević, A.; Mišković, N.; Nad, Đ. Cloud-based mission control of USV fleet: Architecture, implementation and experiments. *Control Eng. Pract.* **2021**, *106*, 104657. [CrossRef]

6. Kang, H.S.; Kim, M.H.; Aramanadka, S.B. Numerical Analysis on Mathieu Instability of a Top-Tensioned Riser in a Dry-Tree Semisubmersible. *J. Offshore Mech. Arct. Eng.* **2020**, *142*, 021701. [CrossRef]
7. Subbulakshmiab, A.; Sundaravadivelub, R. Effects of damping plate position on heave and pitch responses of spar platform with single and double damping plates under regular waves. *Ocean. Eng.* **2021**, *224*, 108719.
8. Liu, Y.; Yoshida, S.; Hu, C.; Sueyoshi, M.; Sun, L.; Gao, J.; Cong, P.; He, G. A reliable open-source package for performance evaluation of floating renewable energy systems in coastal and offshore regions. *Energy Convers. Manag.* **2018**, *174*, 516–536. [CrossRef]
9. Zhang, Q.; Zhang, J.L.; Chemori, A.; Xiang, X.B. Virtual Submerged Floating Operational System for Robotic Manipulation. *Complexity* **2018**, *2018*, 9528313. [CrossRef]
10. Bachynskia, E.; Thysb, M.; Delhayec, V. Dynamic response of a monopile wind turbine in waves: Experimental uncertainty analysis for validation of numerical tools. *Appl. Ocean. Res.* **2019**, *89*, 96–114. [CrossRef]
11. Wang, S.; Xu, S.; Xiang, G.; Guedes Soares, C. An overview of synthetic mooring cables in marine applications. In *Advances in Renewable Energies Offshore*; Taylor & Francis: Abingdon, UK, 2019; pp. 853–863.
12. Gao, Z.; Moan, T. Mooring system analysis of multiple wave energy converters in a farm configuration. In Proceedings of the 8th European Wave and Tidal Energy Conference, Uppsala, Sweden, 7–10 September 2009.
13. Harnois, V. Analysis of Highly Dynamic Mooring Systems: Peak Mooring Loads in Realistic Sea Conditions. Ph.D. Thesis, University of Exeter, Exeter, UK, 2014.
14. Casaubieilh, P.; Thiebaut, F.; Sheng, W.; Retzler, C.; Shaw, M.; Letertre, Y. Performance Improvements of Mooring Systems for Wave Energy Converters. In *Renewable Energies Offshore*; Soares, G., Ed.; European Commission: Brussels, Belgium, 2013; pp. 897–903.
15. Huang, W.; Liu, H.X.; Lian, Y.S.; Li, L.N. Modeling nonlinear time-dependent behaviors of synthetic fiber ropes under cyclic loading. *Ocean. Eng.* **2015**, *109*, 207–216. [CrossRef]
16. Lian, Y.S.; Liu, H.X.; Li, L.N.; Zhang, Y.M. An experimental investigation on the bedding-in behavior of synthetic fiber ropes. *Ocean. Eng.* **2018**, *160*, 368–381. [CrossRef]
17. Davidson, J.; Ringwood, J.V. Mathematical Modelling of Mooring Systems for Wave Energy Converters—A Review. *Energies* **2017**, *10*, 666. [CrossRef]
18. Bosma, B.; Lewis, T.; Brekken, T.; Jouanne, A.V. Wave Tank Testing and Model Validation of an Autonomous Wave Energy Converter. *Energies* **2015**, *8*, 8857–8872. [CrossRef]
19. Thomsen, J.B.; Ferri, F.; Kofoed, J.P. Validation of a Tool for the Initial Dynamic Design of Mooring Systems for Large Floating Wave Energy Converters. *J. Mar. Sci. Eng.* **2017**, *5*, 45. [CrossRef]
20. Sirnivas, S.; Yu, Y.; Hall, M.; Bosma, B. Coupled Mooring Analyses for the WEC-Sim Wave Energy Converter Design Tool. In Proceedings of the International Conference on Offshore Mechanics and Arctic Engineering, Busan, Republic of Korea, 19–24 June 2016; ASME: New York, NY, USA, 2016; Volume 6: Ocean Space Utilization, Ocean Renewable Energy. p. V006T09A023. [CrossRef]
21. Azcona, J.; Munduate, X.; Gonzalez, L.; Nygaard, T.A. Experimental validation of a dynamic mooring lines code with tension and motion measurements of a submerged chain. *Ocean. Eng.* **2017**, *129*, 415–427. [CrossRef]
22. Qiao, D.; Li, B.; Yan, J.; Qin, Y.; Liang, H.; Ning, D. Transient Responses Evaluation of FPSO with Different Failure Scenarios of Mooring Lines. *J. Mar. Sci. Eng.* **2021**, *9*, 103. [CrossRef]
23. Pascoal, R.; Huang, S.; Barltrop, N.; Guedes Soares, C. Equivalent force model for the effect of mooring systems on the horizontal motions. *Appl. Ocean. Res.* **2005**, *27*, 165–172. [CrossRef]
24. Cerveira, F.; Fonseca, N.; Pascoal, R. Mooring systeminfluence on the efficiency of wave energy converters. *Int. J. Mar. Energy* **2013**, *3*, 65–81. [CrossRef]
25. Ran, Z.; Kim, M.H. Nonlinear coupled responses of a tethered spar platform in waves. *Int. J. Offshore Polar Eng.* **1997**, *7*, 111–118.
26. Kang, H.S.; Kim, M.H.; Aramanadka, S.S.B.; Kang, H.Y. Semi-Active Magneto-Rheological Damper to Reduce the Dynamic Response of Top-Tension Risers. In Proceedings of the 23rd International Offshore and Polar Engineering Conference, Anchorage, AK, USA, 30 June–5 July 2013.
27. Bergdahl, L.; Palm, J.; Eskilsson, C.; Lindahl, J. Dynamically Scaled Model Experiment of a Mooring Cable. *J. Mar. Sci. Eng.* **2016**, *4*, 5. [CrossRef]
28. Yang, S.H.; Ringsberg, J.W.; Johnson, E. A comparison of coupled and de-coupled simulation procedures for the fatigue analysis of wave energy converter mooring lines. *Ocean. Eng.* **2016**, *117*, 332–345. [CrossRef]
29. Nguyen, H.P.; Dai, J.; Wang, C.M.; Ang, K.K.; Luong, V.H. Reducing hydroelastic responses of pontoon-type VLFS using vertical elastic mooring lines. *Mar. Struct.* **2018**, *59*, 251–270. [CrossRef]
30. Xiong, L.Z.; Yang, J.M.; Zhao, W.H. Dynamics of a taut mooring line accounting for the embedded anchor chains. *Ocean. Eng.* **2016**, *121*, 403–413. [CrossRef]
31. Xiong, L.Z.; Lu, W.Y.; Li, X.; Guo, X.X. Estimation of damping induced by taut mooring lines. *Int. J. Nav. Archit. Ocean. Eng.* **2020**, *12*, 810–818. [CrossRef]
32. Qiao, D.; Yan, J.; Liang, H.Z.; Ning, D.Z.; Li, B.B.; Ou, J.P. Analysis on snap load characteristics of mooring line in slack-taut process. *Ocean. Eng.* **2020**, *196*, 106807. [CrossRef]

33. Ma, W.; Webster, W.C. *An Analytical Approach to cable Dynamics: Theory and User Manual*; SEA GRANT PROJECT R/OE-26; National Oceanic and Atmospheric Administration: Washington, DC, USA, 1994.
34. Chen, X.H.; Zhang, J.; Johnson, P.; Irani, M. Dynamic analysis of mooring lines with inserted springs. *Appl. Ocean. Res.* **2001**, *23*, 277–284. [CrossRef]
35. Li, J.J.; Xiang, X.B.; Yang, S.L. Robust adaptive neural network control for dynamic positioning of marine vessels with prescribed performance under model uncertainties and input saturation. *Neurocomputing* **2022**, *484*, 1–12. [CrossRef]
36. Garret, G.L. Dynamic Analysis of Slender Rods. *J. Energy Resour. Technol.* **1982**, *104*, 302–306. [CrossRef]
37. Xiang, G.; Xu, S.; Wang, S.; Carlos Soares, C. Comparative study on two different mooring system for a buoy. In Proceedings of the Third International Conference on Renewable Energies Offshore, Lisbon, Portugal, 8–10 October 2018.
38. Chen, X.H.; Ding, Y.; Zhang, J.; Liagre, P.; Niedzwecki, J.; Teigen, P. Coupled dynamic analysis of a mini TLP: Comparison with-measurements. *Ocean. Eng.* **2006**, *33*, 93–117. [CrossRef]
39. Xiang, G.; Guedes Soares, C. Improved Dynamic Modelling of Freely Falling Underwater Cylinder Based on CFD. *Ocean. Eng.* **2020**, *211*, 107538. [CrossRef]
40. Yu, X.C.; Xiang, G.; Collopy, H.; Kong, X. Trajectory Tracking of a Model Rocket Falling into the Towing Tank: Experimental Tests vs. Numerical Simulations. *J. Aerosp. Eng.* **2020**, *33*, 04020056.
41. Xiang, G.; Xiang, X.B. 3D trajectory optimization of the slender body freely falling through water using Cuckoo Search algorithm. *Ocean. Eng.* **2021**, *235*, 109354. [CrossRef]